

The wake and thrust by four side-by-side cylinders at a low Re

Md. Mahbub Alam^{a,*}, Qinmin Zheng^a, Kerry Hourigan^b



^a Institute for Turbulence-Noise-Vibration Interaction and Control, Shenzhen Graduate School, Harbin Institute of Technology, Shenzhen 518055, China

^b Fluids Laboratory for Aeronautical and Industrial Research (FLAIR), Department of Mechanical and Aerospace Engineering, Monash University, Clayton 3800, Australia

ARTICLE INFO

Keywords:

Forces
Wake
Four cylinders
Side-by-side

ABSTRACT

The flow around four identical side-by-side circular cylinders placed normal to the oncoming flow is numerically simulated using the finite volume method (FVM) at a low Reynolds number of 100 based on cylinder diameter D and freestream velocity. How the wake structure, forces, and vortex shedding patterns are contingent on the spacing ratio g^* ($=g/D$, where g is the gap spacing between the cylinders) is studied systemically when g^* varies from 0.0 to 2.0. Based on the intrinsic features of the flow, four distinct flow regimes are identified in the range of g^* examined. The total time-averaged drag force acting on the four cylinders escalates exponentially with a decrease in g^* , as does the lift force, repulsive, on the outer cylinders. The lift forces of the inner cylinders are also repulsive but very weakly sensitive to g^* . The Strouhal number is identical for each of the four cylinders in single body flow, different for the outer and inner cylinders in flip-flopping and quasi-interlocked flows, and again identical for interlocked flow.

1. Introduction

Fluid flow around bluff bodies plays an important role in many engineering fields. Two side-by-side circular cylinders are considered as the simplest model to understand the fluid dynamics around more structures in groups. Fluid dynamics around two side-by-side cylinders has been examined experimentally in a series of articles since Biermann (1930) to until now (e.g., Alam et al., 2003; Alam and Zhou, 2007; Kim and Alam, 2015). Three different flow regimes, depending on the gap spacing ratio g^* ($=g/D$), were identified for the two side-by-side cylinders in a uniform flow of freestream velocity U_∞ , where g is the gap spacing between the cylinders and D is the diameter of a cylinder. They are single-bluff-body ($g^* < 0.2$), flip-flopping ($0.2 \leq g^* < 0.2 \sim 0.7$) and coupled vortex street (CVS, $g^* \geq 0.2 \sim 0.7$) regimes. The ranges are dependent on the Reynolds number $Re = U_\infty D/\nu$ (where ν is the kinematic viscosity), turbulent intensity, etc. The single-bluff-body flow features a single wake with a predominant Strouhal number $St=fD/U_\infty$, where f is the vortex shedding frequency (e.g., Zdravkovich, 1977; Alam et al., 2003). In terms of the wake dynamics, the two cylinders behave like one bluff body. In the flip-flopping flow, the gap flow between the cylinders spontaneously flip-flops randomly, forming asymmetric (narrow and wide) wakes where the gap is biased or symmetric wakes where the gap flow is straight. While the narrow and wide wakes correspond to a high and a low St , respectively, or (e.g. Bearman and Wadcock, 1973), the symmetric wakes correspond to an identical St that is equal to that of a single isolated cylinder (Kim and Durbin, 1988; Moretti, 1993; Alam et al., 2003). Two symmetric coupled wakes of the same St are generated in the CVS flow, displaying either inphase or antiphase vortex streets (e.g., Kamemoto, 1976; Meneghini et al., 2001). Alam et al. (2003) found that the intermittent presence of the CVS flow in the flip-flopping regime results in the symmetric wakes, with their duration being shorter as g^* is reduced from 1.2 to

* Corresponding author.

E-mail addresses: alam28@yahoo.com, alam@hitsz.edu.cn (Md. M. Alam).

0.2. Afgan et al. (2011) investigated the flow around two side-by-side cylinders using dynamic Smagorinsky large eddy simulation (LES), with the spacing ratio of $0.25 \leq g^* \leq 4.0$ at a $Re=3000$. They observed bistable flow for $0.25 \leq g^* \leq 0.75$. On the other hand, Carini et al. (2014) for $50 < Re \leq 90$ detected the bistable flow at $0.6 \leq g^* \leq 1.4$, suggesting that the bistable flow at a lower Re occurs for a higher g^* range.

While a number of similar studies have been carried out for two circular cylinders in side-by-side arrangement, somewhat less attention has been paid to examine the fluid dynamics around more than two cylinders, where a much more complex flow is involved. Some features of flow around multiple cylinders can be predicted based on the fluid dynamics knowledge of two cylinders, but some are not, requiring investigation on more than two cylinders.

While more cylinders placed in tandem do not influence the flow around the upstream cylinders much, those in side-by-side configuration make the wake very complex due to interactions between adjacent shear layers, between adjacent vortices and between adjacent wakes. In the past, three circular cylinders in side-by-side arrangement have been examined experimentally at $Re=1.0 \times 10^4 \sim 3.2 \times 10^4$ by Kumada et al. (1984). They observed four typical flow structures. The three cylinders behaved like a single bluff body with one vortex street at $g^*=0.0 \sim 0.125$. For $g^*=0.125 \sim 0.35$, the two gap flows swerving to one side form a narrow and a wide wake. The two gap flows were deflected towards the freestream side shear layers, respectively, forming a wide wake behind the middle cylinder and narrow wakes behind the outer cylinders. Though much different and complex flow physics was observed in three side-by-side circular cylinders compared to two side-by-side cylinders, three side-by-side cylinders have not been studied extensively, perhaps because of cylinder blockage issues in wind tunnels. Now that computation techniques have been improved, researchers have set their focus on more and more cylinders in a group. For example, Kumar et al. (2008) investigated the flow around a row of nine square prisms at a low-Reynolds number ($Re=80$) for $g^*=0.3 \sim 12.0$, using the Lattice-Boltzmann method. Three different flow regimes were revealed by the vorticity field and drag coefficient signal: synchronized flow, quasi-periodic flow, and chaotic flow. However, to our knowledge, a systematic study of four side-by-side circular cylinders at low Re does not seem to have undertaken before. The four side-by-side cylinders can also be regarded as a simple model of four fingers of a swimmer's hand. Of course, the fingers of a hand are of different diameters and different length. We are interested to know how the fluid dynamics around four fingers of identical diameters is dependent on the gap spacing.

The objective of this investigation is to study the hydrodynamics of four cylinders representing the four fingers of a hand at a low $Re=100$. Flow structures, St , and forces are examined in detail with a change in g^* from 0.0 to 2.0.

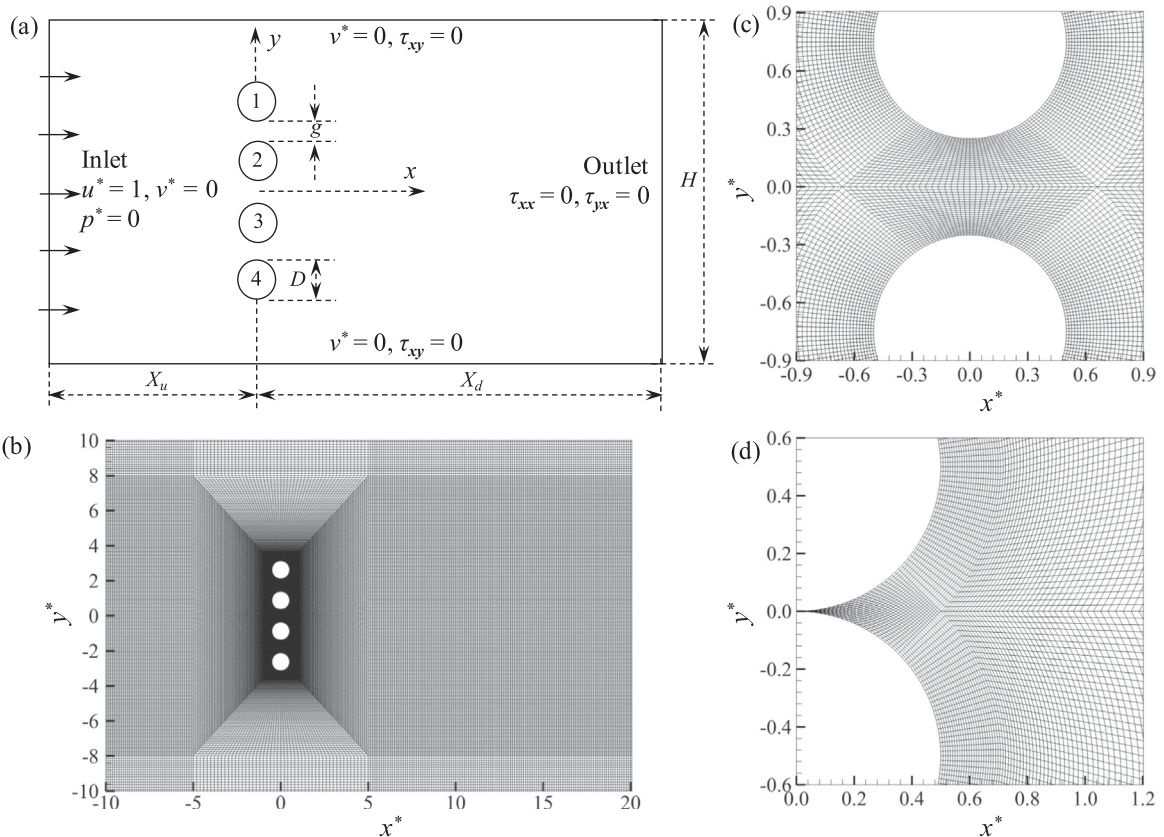


Fig. 1. (a) Sketch of computational domain and boundary conditions. (b) Grid distribution around four side-by-side cylinders. Zoom-in views of grid distributions around and in the gap between two cylinders at (c) $g^*=0.5$ and (d) $g^*=0.0$.

Table 1
Results of grid and time-step independence test. $Re = 100$.

Time step	Forces and St	Number of nodes, N_n				
		4.0×10^4	4.7×10^4	6.9×10^4	8.2×10^4	11.0×10^4
0.05	C_D	1.374	1.370	1.369	1.367	1.365
	$(C_L)_{\max}$	0.316	0.304	0.299	0.279	0.275
	St	0.168	0.163	0.159	0.157	0.157
0.01	C_D	1.379	1.376	1.372	1.370	1.367
	$(C_L)_{\max}$	0.309	0.296	0.296	0.288	0.286
	St	0.174	0.165	0.165	0.165	0.165
0.005	C_D	1.382	1.380	1.376	1.372	1.370
	$(C_L)_{\max}$	0.306	0.292	0.294	0.291	0.288
	St	0.176	0.173	0.168	0.166	0.166
0.001	C_D	1.380	1.382	1.375	1.370	1.372
	$(C_L)_{\max}$	0.306	0.290	0.295	0.291	0.287
	St	0.175	0.170	0.167	0.166	0.167

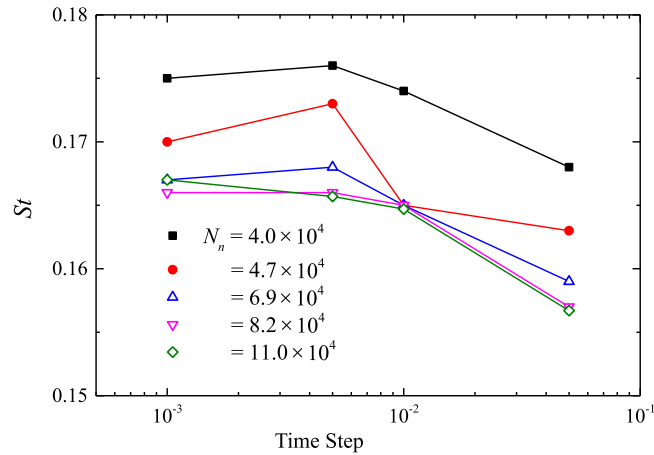


Fig. 2. Dependence of Strouhal number St on N_n and time-step.

Table 2
Comparison of results for a single cylinder at $Re=100$.

	C_D	$(C_L)_{\max}$	St
Present	1.372	0.296	0.165
Williamson (1991), Exp.	–	–	0.164
Norberg (2003), Exp.	–	0.25–0.42	0.168
Meneghini et al. (2001), CFD	1.37	–	0.165
Bourguet and Jacono (2014), CFD	1.32	0.32	0.164
Ding et al. (2007), CFD	1.36	0.287	0.166
Braza et al. (1986), CFD	1.28	0.29	0.16
Kang et al. (1999), CFD	1.32	0.32	0.165
Shiels et al. (2001), CFD	1.33	0.30	0.167
Shen et al. (2009), CFD	1.38	0.33	0.166

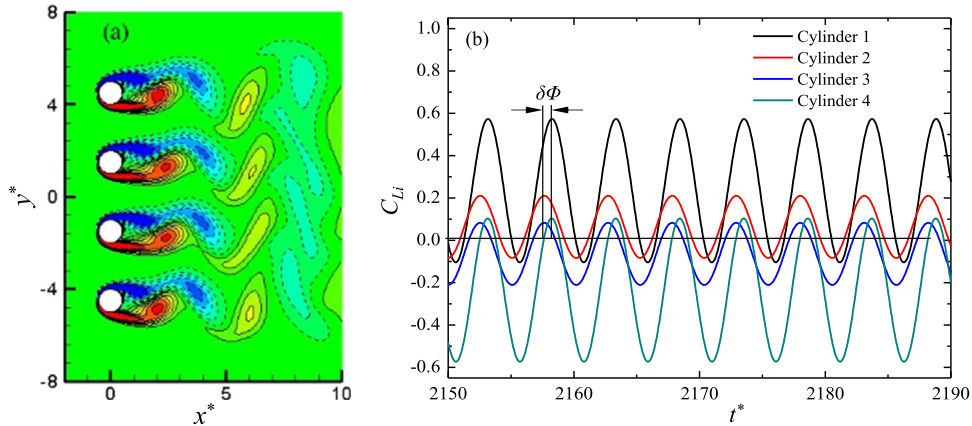
2. Computational details

2.1. Numerical method

The governing equations for an unsteady, viscous, laminar and incompressible fluid flow with constant properties are the continuity and momentum equations expressed in Cartesian coordinate as

Table 3Effects of mesh resolution on the flow around four cylinders at $g^* = 0.25$.

Mesh	Time step		St	C_L'	C_L	C_D
Case 1: $N_n = 25.7 \times 10^4$	0.01	Cylinder 1	0.053	0.028	1.093	1.692
		Cylinder 2	0.053	0.027	0.131	2.941
Case 2: $N_n = 45.3 \times 10^4$	0.005	Cylinder 1	0.054	0.027	1.100	1.688
		Cylinder 2	0.054	0.027	0.128	2.912

**Fig. 3.** (a) Instantaneous vorticity contours and (b) time-histories of lift coefficients for $g^* = 2.0$. Interlocked flow.

$$\frac{\partial \mathbf{u}^*}{\partial t^*} + (\mathbf{u}^* \cdot \nabla) \mathbf{u}^* = -\nabla p^* + \frac{1}{Re} \nabla^2 \mathbf{u}^*,$$

and

$$\nabla \cdot \mathbf{u}^* = 0,$$

where the freestream velocity U_∞ and the cylinder diameter D are used as the reference speed and reference length, respectively, to normalize the parameters. $\mathbf{u}^* = (u^*, v^*)$ is the normalized velocity field, t^* is the non-dimensional time, and p^* is the normalized static pressure. The differential equations are coupled and solved for the unknown p^* , u^* and v^* . The gravity force is excluded. The computations are performed using the Ansys-Fluent solver based on the finite volume method. While a standard scheme and a second-order upwind scheme are used to discretize pressure and velocity, respectively, the first-order implicit formulation is used for time discretization. On the other hand, the coupling between the pressure and velocity fields is achieved using the SIMPLE technique. $Re=100$ is adopted in the simulation. Grid and time independence tests were performed first. Regular fluctuation in lift force with time was generally adopted as the judging criterion for the convergence of the simulation.

Fig. 1(a) shows a schematic diagram of the computation domain, cylinder arrangement, definitions of symbols and boundary conditions. The gap width between the cylinders is defined by g , normalized as $g^* = g/D$. A Cartesian coordinate system is employed such that the origin is at the midpoint between the centers of the two middle cylinders, with x - and y -axis along the streamwise and lateral directions, respectively. The computational domain size is chosen as $X_u = 10.0D$, $X_d = 25.0D$ and $H = 80.0D$ (Sohankar et al., 1998; Kumar et al., 2008; Sewatkar et al., 2011). An O-xy grid system near the cylinders and a rectangular-grid system away from the cylinders were used (Fig. 1b). The number of cells for the O-grid system was 200 in the transverse direction. Therefore, a total of 200 points were on the cylinder surface. The first level of mesh spacing near the cylinder surface is set to be $0.005D$ for an adequate resolution of the boundary layer, with the mesh spacing increasing with an expansion rate of 1.029 in the radial direction (Fig. 1b). Though unstructured meshes are widely adopted for complex models, structured meshes are used for the present simple and symmetric models (Afgan et al., 2011; Zhao and Cheng, 2014; Tong et al., 2015; Alam, 2016). Fig. 1(c, d) presents zoom-in views of grid distributions around and in the gap between two cylinders at $g^* = 0.5$ and 0.0 . The mesh distributions for both cases are similar, with a slight difference at the gap for $g^* = 0.0$, where the mesh skewness is relatively larger.

On lateral surfaces, the velocity component normal to the boundaries and the stress vector component along the boundaries are set to zero (Prasanth and Mittal 2008). The no-slip boundary condition is applied at the cylinder walls. All simulations start with the initial velocity $u^* = 1.0$, $v^* = 0$. The simulations were performed for $g^* = 0.0, 0.25, 0.5, 0.75, 1.0, 1.25, 1.5$, and 2.0 ; and vorticity patterns, shedding frequencies, drag and lift forces were extracted and presented in this paper. While Re for a swimmer's finger varies and the flow around the fingers is highly three-dimensional, $Re=100$ is chosen arbitrarily in the laminar flow regime (Williamson, 1996) so that a two-dimensional simulation can be adopted to reduce computation cost. Note that the strong vortex shedding occurs at $Re=100$, which also occurs for even much higher Re ($< 10^5$, Zdravkovich, 1997).

Time-averaged lift and drag coefficients (C_L and C_D , respectively) and fluctuating lift coefficient C_L' are defined as:

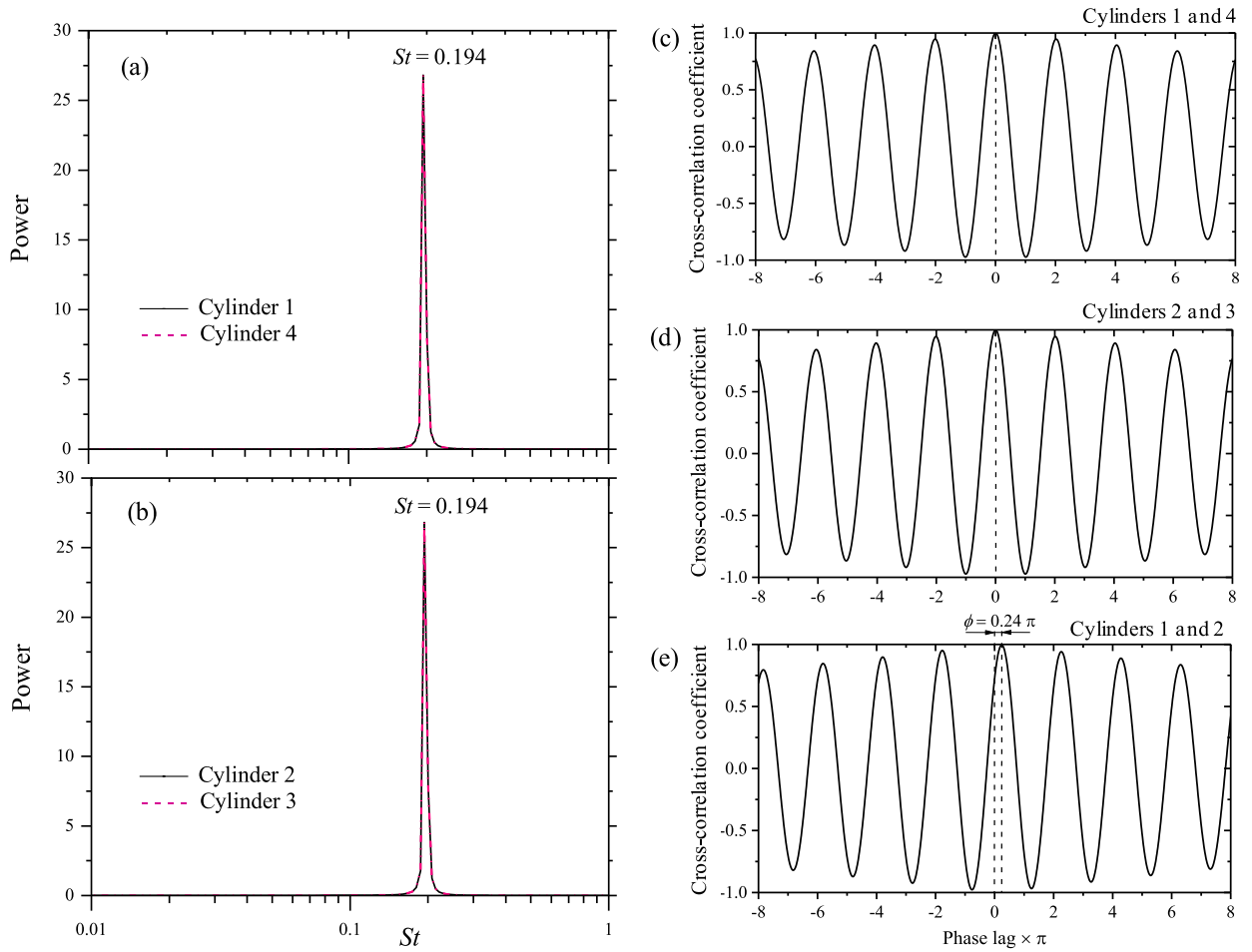


Fig. 4. (a, b) Power spectral density functions of fluctuating lift coefficients. (c, d, e) Cross correlation coefficient between fluctuating lift forces. The phase lag is calculated based on $St = 0.194$. $g^* = 2.0$. Interlocked flow.

$$C_D = \frac{2F_D}{\rho U_\infty^2 D},$$

$$C_L = \frac{2F_L}{\rho U_\infty^2 D},$$

and

$$C'_L = \frac{2F'_L}{\rho U_\infty^2 D},$$

where F_L and F_D , respectively, refer to time-averaged lift and drag forces, and F'_L is the r.m.s of the lift force.

2.2. Validation of the numerical model

Flow past a single circular cylinder at $Re=100$ was simulated first to validate the numerical model used in the present work. The effect of mesh resolution on the flow around a single isolated cylinder was investigated before the extensive simulations while the computational domain and mesh distribution are defined to be similar to that of four side-by-side cylinders. Five different meshes (node numbers $N_n = 4.0 \times 10^4$, 4.7×10^4 , 6.9×10^4 , 8.2×10^4 , 11.0×10^4) for a single cylinder were tested with a decreasing time step of 0.05, 0.01, 0.005 and 0.001. Details of the integral outputs (e.g., St , C_D and lift amplitude $(C_L)_{\max}$) are presented in Table 1. The St data in Table 1 are plotted as a function of N_n and time-step in Fig. 2. The computational domain size was identical for the five meshes with $X_u = 10.0D$, $X_d = 25.0D$ and blockage ratio = 5.0%. Evidently, the forces and St results converged for $N_n = 6.9 \times 10^4$ with time step of 0.01 at which the largest deviation between the meshes $N_n = 6.9 \times 10^4$ and 11.0×10^4 is about 3.4% for $(C_L)_{\max}$. Further, the largest deviation between time steps 0.01 and 0.001 with $N_n = 6.9 \times 10^4$ occurs for St , about 1.2%. This establishes the adequacy of $N_n = 6.9 \times 10^4$ and time step = 0.01 for computing the flow past a single isolated cylinder, where the corresponding Courant number

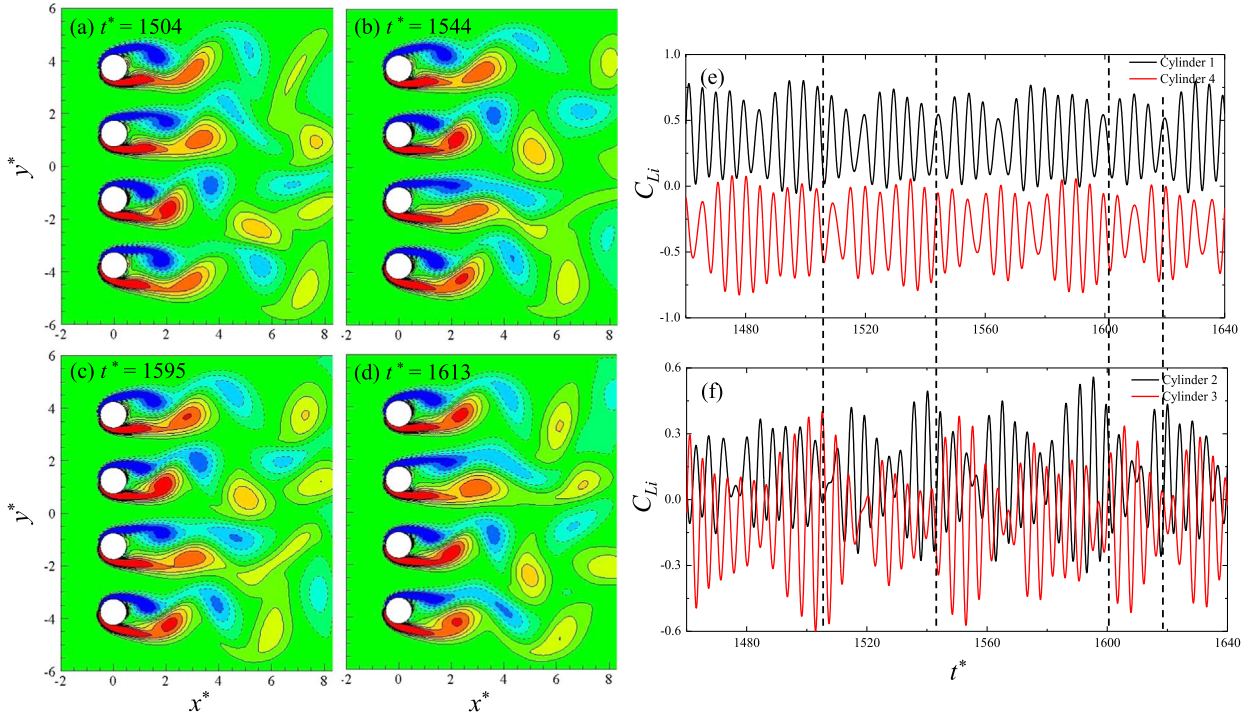


Fig. 5. (a–d) Instantaneous vorticity contours and (e, f) time-histories of lift coefficients. $g^* = 1.5$. Quasi-interlocked flow.

was less than 0.2 in the whole computational domain.

Table 2 compares C_D , $(C_L)_{\max}$ and St with those in the literature, stating a good agreement. The experimental $(C_L)_{\max}$ results by Norberg (2003) have a range, depending on the measured axial length of the cylinder; $(C_L)_{\max}$ gets smaller for a larger length. The departure of the present results from the mean values in the literature is less than 2.3%, 3.4%, and 0.1% for C_D , $(C_L)_{\max}$ and St , respectively.

2.3. Validation of mesh resolution for four cylinders

Validations of the mesh resolution and time step for the flow around four side-by-side cylinders are conducted for a small $g^* (=0.25)$ at which there are appreciable flows through the gaps. As discussed above, the mesh density and time-step for the single cylinder flow are validated as 6.9×10^4 and 0.01, respectively. With similar grid density employed for the four side-by-side cylinders, the total grid number is 25.7×10^4 for $g^* = 0.25$. The total grid number is increased to 45.3×10^4 , corresponding to a 176% increase in the grid density. The time step is thus reduced to half (0.005). The results for $N_r = 25.7 \times 10^4$ and 45.3×10^4 are presented as cases 1 and 2 in Table 3. Note that, the results for the cylinders 1 and 4 (or cylinders 2 and 3) are identical; those for the cylinders 1 and 2 only are thus presented. It is observed that St and C'_L do not change between the two cases, and the largest differences in C_L and C_D between the two cases are 2.34% and 0.99%, respectively. Therefore, the grid density employed is large enough to resolve the flow field around four cylinders.

3. Results and discussion

3.1. Wake structure and force signals

$g^* = 2.0$ is simulated first and then reduced to 0.0 successively. When g^* was varied from 2.0 to 0.0, four distinct flow regimes are observed, namely interlocked flow, quasi-interlocked flow, flip-flopping flow and single-body flow. Each of them has distinct characteristics as discussed below.

3.1.1. Interlocked flow ($g^* \geq 2.0$)

The interlocked flow occurs at $g^* \geq 2.0$. Each of the four cylinders generates a vortex street that resembles a single isolated cylinder's street (Fig. 3a). The four streets and the shedding from the cylinders are, however, interlocked in an inphase fashion. The inphase flow can be confirmed by the time-histories of lift forces of the four cylinders (Fig. 3b). The two outer cylinders (cylinders 1 and 4) have the same amplitude of lift, larger than that of the inner cylinders (cylinders 2 and 3). The time-averaged value of the lift is, however, positive for the upper two (cylinders 1 and 2) and negative for the lower two (cylinders 3 and 4), implying that all the cylinders experience a repulsive lift force about the centerline $y^* = 0$ of the four cylinders. While the lift fluctuations of the two inner

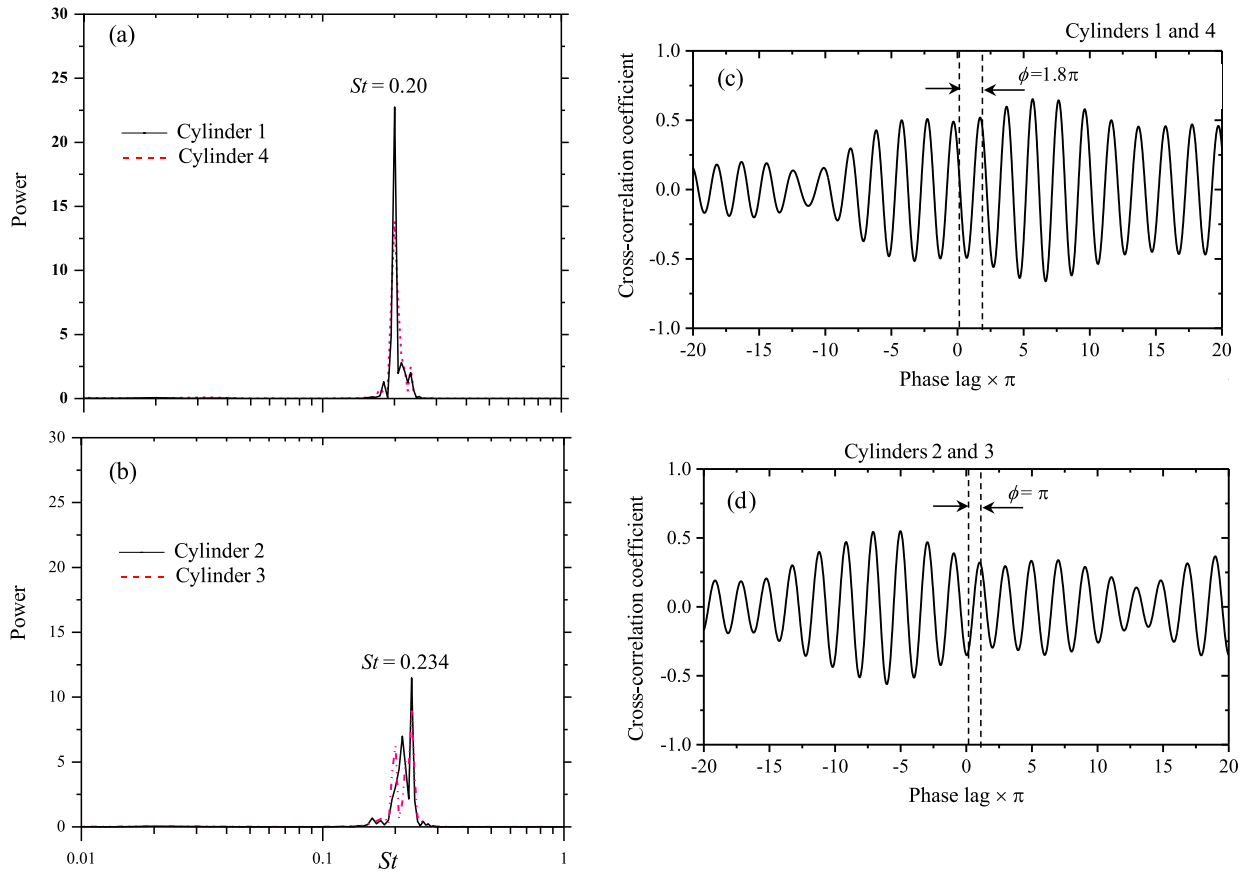


Fig. 6. (a, b) Power spectral density functions of fluctuating lift coefficients. (c, d) Cross correlation coefficient between fluctuating lift forces. The phase lag is calculated based on $St = 0.20$ for (c) and 0.23 for (d). $g^* = 1.5$. Quasi-interlocked flow.

cylinders are exactly inphase, those of the two outer cylinders are also inphase but with a phase lag $\delta\phi = 43^\circ$ with respect to the inner cylinders. Power spectral density functions of fluctuating lift of the four cylinders presented in Fig. 4(a, b) reveal that the four cylinders have the same shedding frequency corresponding to a $St = 0.194$, which is about 18% higher than that for an isolated cylinder. In order to further corroborate the vortex shedding phase relationship between the cylinders, cross-correlation coefficients of fluctuating lift between the outer cylinders (Fig. 4c), between the inner cylinders (Fig. 4d), and between an inner and an outer cylinder (Fig. 4e) are estimated as a function of the phase lag. The correlation coefficient between the outer cylinders becomes a maximum of 1.0 when the phase lag is zero, implying that the vortex shedding from the outer cylinders is synchronous (Fig. 4c); similarly, this is the case for the vortex shedding from the inner cylinders (Fig. 4d). For both cases (Fig. 4c, d), as the phase lag is increased/decreased to $\pm 2\pi$, the value of the coefficient is comparable to that at zero phase lag, indicating that the vortex sheddings from the cylinders are interlocked and well correlated. On the other hand, the correlation coefficient between an outer and inner cylinder (Fig. 4e) is maximum at a phase lag of $0.24\pi (=43^\circ)$; that is, the shedding from the inner cylinders leads that from the outer cylinders by 0.24π .

3.1.2. Quasi-interlocked flow ($1.0 \leq g^* < 2.0$)

When g^* decreases to $1.0 \leq g^* < 2.0$, a beat-like variation in lift forces is observed. Fig. 5 displays instantaneous vorticity contours and time-histories of lift forces at $g^* = 1.5$, demonstrating that the sheddings from the two outer cylinders, with an identical frequency, are interlocked and almost inphase, and those from the other two, with another identical frequency, larger than the prior, are interlocked antiphase. Although the two outer or inner cylinders are interlocked with each other, the outer and inner cylinders are not interlocked as they have different frequencies, $St = 0.20$ and 0.234 for the outer and inner cylinders, respectively. The flow is thus called quasi-interlocked. Due to the difference in the shedding frequencies between the outer and inner cylinders, the four cylinders may have a different instantaneous phase lag in their sheddings, including inphase (synchronous) for the upper two cylinders and antiphase (asynchronous) for the lower two (Fig. 5a), and vice versa, the upper two antiphase and the lower two inphase (Fig. 5b, c). For the former pattern (Fig. 5a), the fluctuation in the lift is the greatest for cylinder 3 as the sheddings from the two sides of either gap concerned with the cylinder is coupled, synchronous ($\approx 0^\circ$ phase lag); it is the smallest for cylinder 2 as the sheddings are coupled, synchronous ($\approx 0^\circ$ phase lag) from the lower gap of the cylinder and asynchronous ($\approx 180^\circ$ phase lag) from the upper gap. On the other hand, for the latter pattern (Fig. 5b, c), cylinder 2 accompanied by synchronous shedding from the each of

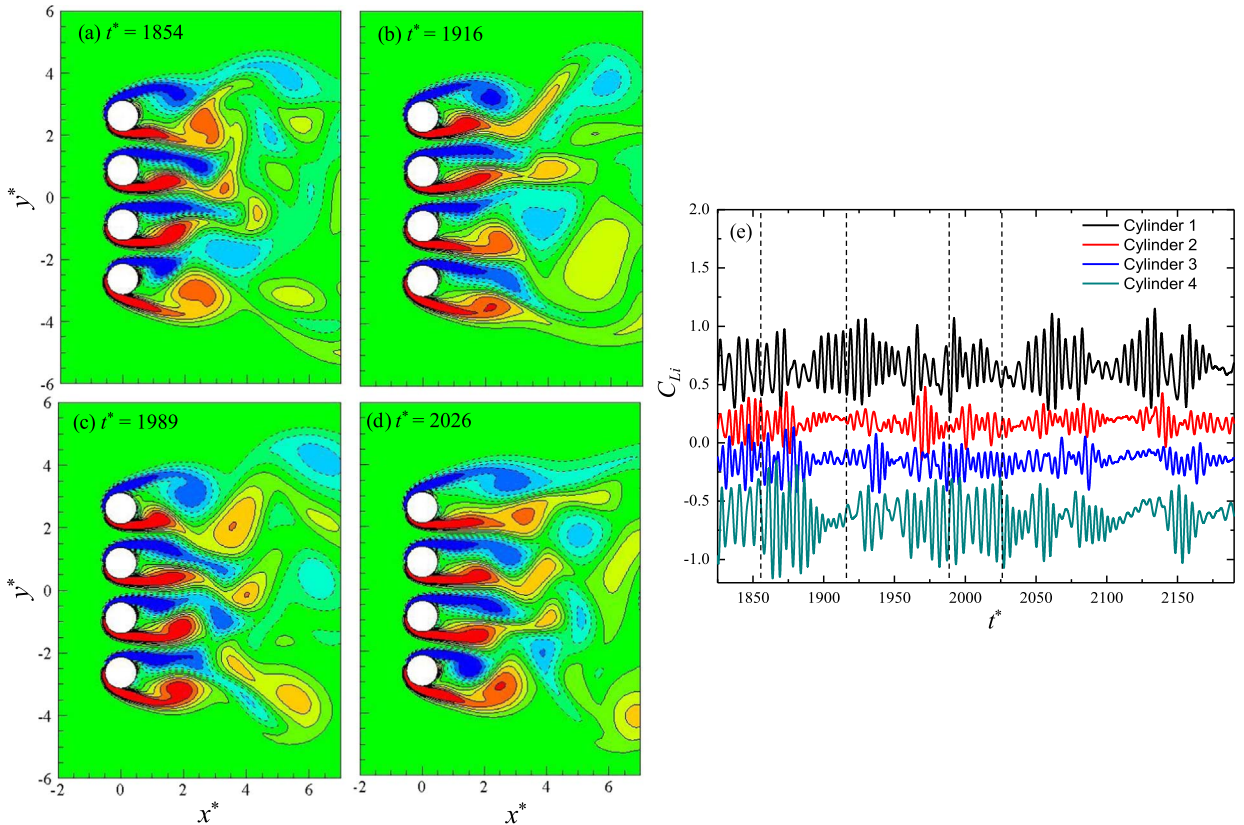


Fig. 7. (a–d) Instantaneous vorticity contours and (e) time-histories of lift coefficients. $g^* = 0.75$. Flip-flopping flow.

the two adjacent gaps experiences a larger fluctuating lift (Fig. 5e, f).

Interestingly, when the sheddings from the lower two gaps or the upper two gaps are coupled and the sheddings from the other gap are of about 90° phase lag, there will be a tendency of the sheddings from the latter gap to be coupled. In this case, the shedding from the outer side of the associated inner cylinder slows down (e.g., cylinder 2, Fig. 5a; cylinder 3, Fig. 5b; cylinder 3, Fig. 5c; cylinder 2, Fig. 5d). In such a case, the corresponding cylinder will have a wider wake and smaller fluctuation in the lift; see the lift of the corresponding cylinder in Fig. 5(f).

The difference in frequencies also makes the time series of the lift forces have a beat-like change with varying amplitude (Fig. 5e, f). The two inner cylinders experience an undulation in their lift forces larger than for the two outer cylinders. This is because the two inner cylinders have the chance of coupled shedding from the two adjacent gaps. For the outer cylinders, coupled shedding may happen only from one gap concerned.

The power spectra of the fluctuating lift of the cylinders confirm that the two outer cylinders have identical $St (=0.20)$, which is smaller than that ($=0.234$) for the inner cylinders (Fig. 6a, b). The shapes of the power spectrum peaks for the outer and inner cylinders are different, skewed right and left for the outer and inner cylinders, respectively; on the other hand, those for the interlocked flow were symmetric (Fig. 4a, b). The skewness of the peaks bears the signature of the interaction between the low- and high-frequency vortices from the outer and inner cylinders, respectively. In other words, the outer cylinder shedding is interacted by the inner cylinder shedding and vice versa. The peak is more skewed for the inner cylinders than the outer cylinders, suggesting that an inner cylinder wake is more interacted by the outer cylinder wake than it interacts. The information is also reflected from Fig. 5 where an inner cylinder wake or lift changes more irregularly with time than an outer cylinder. Because of the inner cylinder interaction to the outer cylinders, the correlation coefficient between the two outer cylinders cannot reach 1.0, the maximum magnitude being 0.65. On the contrary, the more interaction of the outer cylinders with the inner cylinders further deteriorates the correlation coefficient for the inner cylinders to be 0.52 maximum. The shedding phase lag is 1.8π (almost inphase) between the outer cylinders and π between the inner cylinders. The variation in the correlation coefficient with the phase lag for either case (Fig. 6c, d) has a beat-like change, with the lift forces of the cylinders having the same (Fig. 5e, f). The correlation between inner and outer cylinders is not presented as an outer and an inner cylinder have different shedding frequencies.

3.1.3. Flip-flopping flow ($0.25 < g^* < 1.0$)

Wakes being narrower or wider than that of a single isolated cylinder appear behind the four cylinders when $0.25 < g^* < 1.0$. The narrow and wide wakes switch from one to the other randomly as can be seen from the vorticity patterns and lift signals shown in Fig. 7 for $g^* = 0.75$. The two outer cylinders feature wide wakes (Fig. 7a, c), larger lift amplitudes (Fig. 7e), stronger shedding

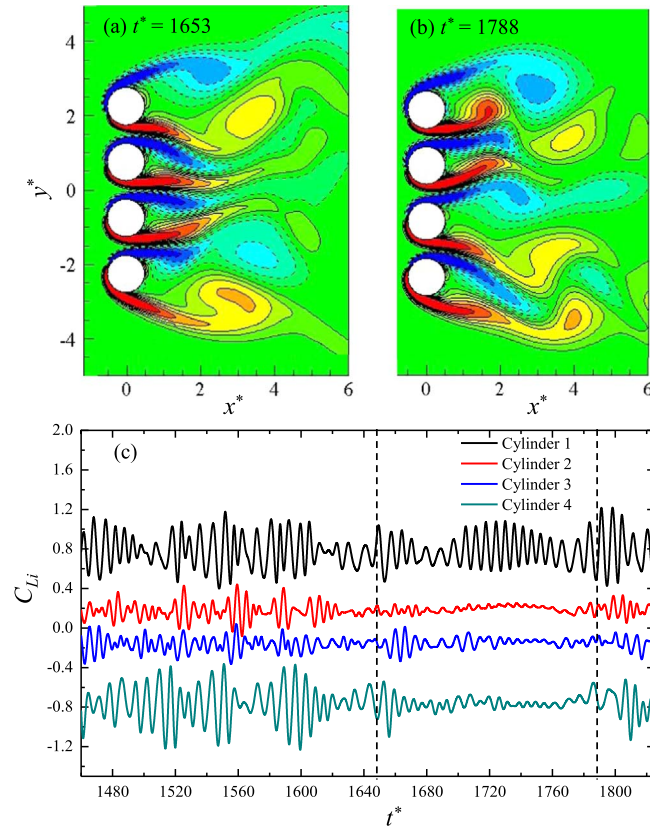


Fig. 8. (a–b) Instantaneous vorticity contours and (c) time-histories of lift coefficients. $g^* = 0.5$. Flip-flopping flow.

occurring alternately, coupled sheddings from the gap concerned, while the inner cylinders have opposite features: narrow wakes, smaller lift amplitudes, and weaker shedding not alternating exactly. The larger amplitude of the lift for the outer cylinders largely results from the alternate and coupled sheddings from the gaps concerned. A strong alternating shedding appearing only for cylinder 1 (Fig. 7b) and only for cylinder 4 (Fig. 7d) engenders again a large amplitude of lift for the respective cylinders. The observation implies that the outer and inner cylinders largely undergo respectively larger and smaller lift amplitudes due to an alternating shedding for the former and an almost symmetric shedding for the latter. The symmetric sheddings from the inner cylinders are more conspicuous at a smaller $g^* = 0.5$ (Fig. 8). Comparing Figs. 7 and 8, it can be concluded that the widths of wide and narrow wakes swell and shrink, respectively, with g^* decreasing. The four wakes transmute to a single wake downstream. A large vortex behind the cylinders forms through an amalgamation process. As the formation of this vortex occurs away from the cylinders, its influence on the lift forces is expected to be small. Alam and Zhou (2013) for two side-by-side square cylinders showed that narrow and wide wakes in flip-flopping flow merge into single one through a vortex amalgamation process. Alam et al. (2011) observed the smallest amplitude of lift forces on the cylinders for the flip-flopping flow.

The power spectra at $g^* = 0.75$ show peaks at $St = 0.154$ and 0.194 for the outer cylinders and $St = 0.214$ for the inner cylinders; again the inner cylinders have a greater St corresponding to the persistent narrow wake (Fig. 9). The St peaks are broad banded due to the flip-flopping of the flow and vigorous interaction between the wakes. A detailed examination of flow and lift forces of the outer cylinders divulged that the outer cylinders largely experience two modes of the wake: a wide wake (for example Fig. 7a, the outer gap flows biased inward) corresponding to $St = 0.154$, and a relatively narrow wake (for example Fig. 7b, the outer gap flows biased outward) corresponding to $St = 0.194$. As a consequence of vigorous interactions and flip-flopping, the correlation coefficient is small, less than 0.3 for either case (Fig. 9c, d). While the shedding phase lag between the outer cylinders is 0.8π (almost antiphase), that between the inner cylinders is 0.21π (almost inphase).

3.1.4. Single-body flow ($g^* \leq 0.25$)

The four cylinders act as a combined bluff body where vortex sheddings occur only from the freestream sides of the outer cylinders, forming one Karman wake of a much smaller St (Fig. 10a). The gap flows are too weak to form vortices and interfere with the freestream side shear layers. However, they move freely up and down following the sheddings from the freestream sides. Lift histories of the four cylinders are regular and of constant amplitude and frequency (Fig. 10b, c). The lift amplitude is, however, larger for the outer cylinders than the inner. Overall, observing the lift signals, it can be concluded that time-averaged lift force is always repulsive about $y^* = 0$, decreasing with increasing g^* .

The St identified from the power spectra of lift forces is 0.053 for all the cylinders. The St peaks are now sharp. A small peak at

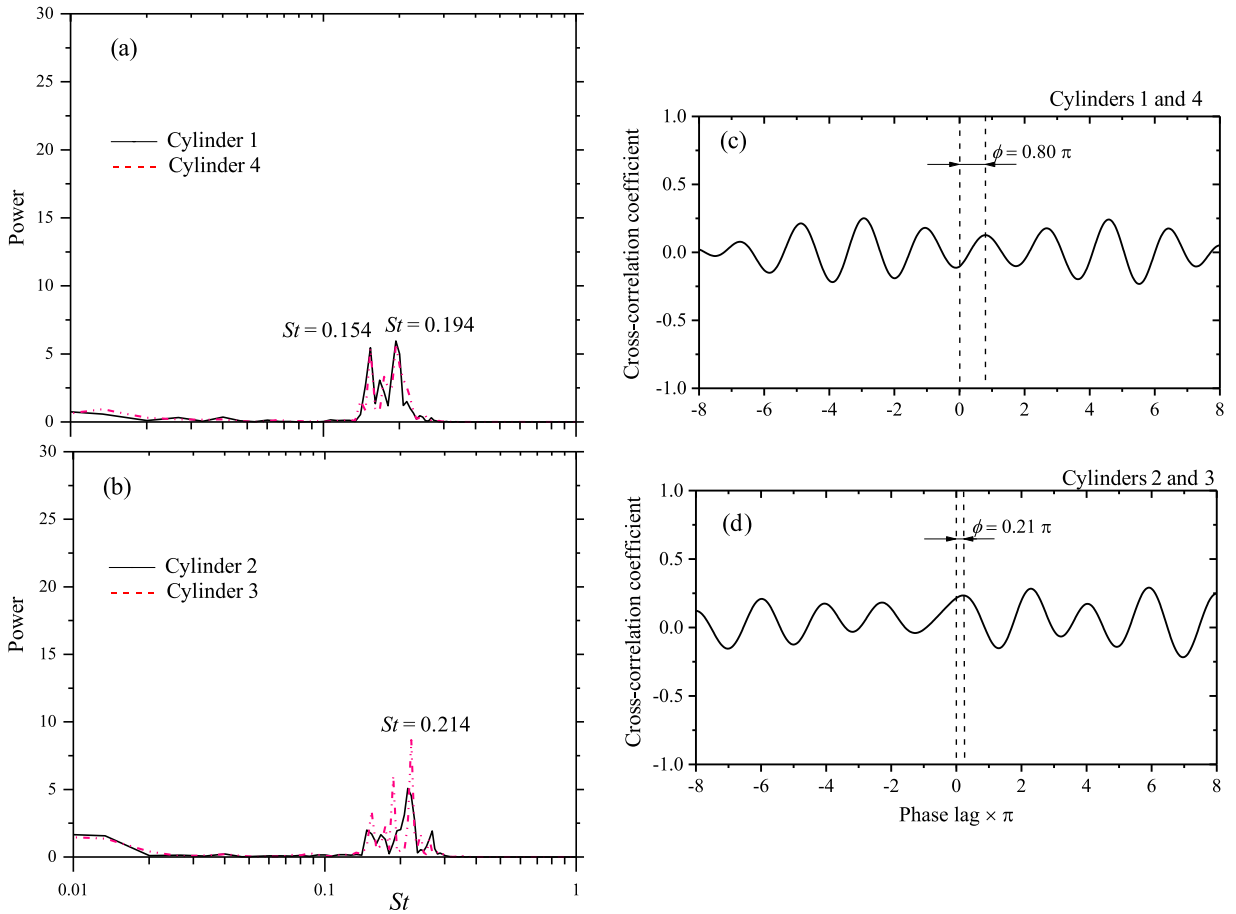


Fig. 9. (a, b) Power spectral density functions of fluctuating lift coefficients. (c, d) Cross correlation coefficient between fluctuating lift forces. The phase lag is calculated based on $St = 0.174 = (0.154 + 0.194)/2$ for (c) and 0.214 for (d). $g^* = 0.75$. Flip-flopping flow.

$St = 0.106$ represents the second harmonics of $St = 0.053$. The correlation coefficient of the wakes between the cylinders rises to about 1.0 (Fig. 11c, d, e) as the interaction of the gap flows to the shedding from the freestream sides is rather weak compared to its counterpart in flip-flopping flow. Interestingly, the phase lag of the wakes between any two of the four cylinders is ≈ 0.0 , confirming that the four cylinders indeed are united, leading to an effective single body wake. At $g^* = 0.0$, considering the four cylinders as one single body, the effective St based on the total height ($=4.0D$) is estimated to be about 0.212, larger than that of the single isolated cylinder ($St = 0.168$, Table 1). The difference might be connected to the effective cross-section modified from circular to a large aspect ratio cylinder at $g^* = 0.0$. Similar observation was made by Alam et al. (2011) for the flow around two side-by-side square cylinders at $g^* = 0.02$. While the effective St for the two cylinders at $g^* = 0.02$ was 0.141, the St for the single isolated square cylinder was 0.128.

3.2. Hydrodynamic forces and shedding frequencies

More detailed C_D , C_L , C'_L , and St of the individual cylinders as a function of g^* are presented in Fig. 12. Flow regimes are marked at the top of each figure. This also reveals how the forces and St are connected to different flow regimes. The outer cylinders undergo the same C_D , as do the two inner cylinders. The C_D of the latter cylinders is, however, considerably larger in the single-body and flip-flopping regimes. The larger C_D is attributed to the fact that the inner cylinders are largely accompanied by narrow wakes with smaller formation length (Figs. 10a, 8a, 7a–d). The slight difference in C_D for the two inner cylinders for $g^* = 0.5$ might be due to the irregular feature of flow caused by the flip-flopping of the gap flows. While the C_D of the two inner cylinders wanes exponentially with g^* , that of the outer cylinders wanes, augments, and declines in the single-body, flip-flopping and quasi-interlocked regimes, respectively. The exponential behavior of C_D of the inner cylinders, different from that of the outer cylinders, results from the fact that either side of an inner cylinder is subjected to the gap flows whose nature is highly sensitive to g^* ; on the other hand, the outer side of an outer cylinder is always subjected to the freestream flow.

C_L is positive for the upper two cylinders and negative for the lower two cylinders, implying that lift forces on the cylinders are always repulsive. The magnitude of C_L for the outer cylinders is more sensitive to g^* and larger than that for the inner cylinders. Since C_L is characterized by the difference in nature of the flow on the two sides of a cylinder, an outer cylinder experiences a larger C_L magnitude, as the two sides of the cylinder are subjected to two different flows (freestream and gap flows), respectively. Again, C_L

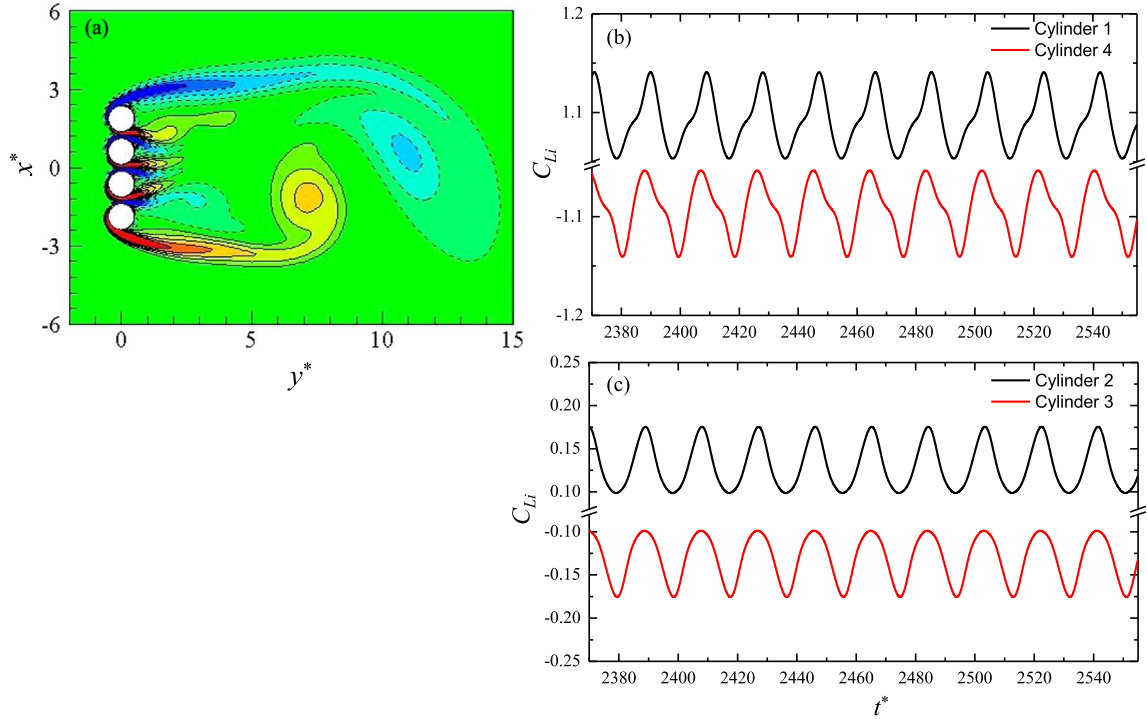


Fig. 10. (a) Instantaneous vorticity contours and (b, c) time-histories of lift coefficients. $g^* = 0.25$. Single bluff-body flow.

magnitude characterizes the flow regimes: large for the outer cylinders in single-body flow where there is strong vortex shedding only from the freestream sides of the outer cylinders (Fig. 10a); mild in flip-flopping flow where an improvement in the gap flow lessens the difference in the flows over the outer and inner sides (Fig. 7a-d); and small in quasi-interlocked flow due to a further improvement in the gap flow (Fig. 5a-d).

In general, the outer cylinders have a C_L' greater than the inner cylinders (Fig. 12c); the difference might be attributed to the strong vortex shedding from the freestream sides. The difference is almost unchanged in the flip-flopping and quasi-interlocked flows but swells in the interlocked flow. It will be shown later that the inner cylinders shed vortices at a higher frequency than the outer cylinders in flip-flopping and quasi-interlocked flows, but the inner cylinder shedding locks-in to the outer cylinder shedding, deviating from its natural shedding. C_L' is thus reduced for the inner cylinders in the interlocked flow ($g^* = 2.0$).

St distributions shown in Fig. 12(d) reflect that St is small and identical ($St \approx 0.05$) for the four cylinders in single body flow, increases (being different for the outer and inner cylinders) with g^* in flip-flopping flow, and large (yet remaining different for the outer and inner cylinders) for the quasi-interlocked flow. The difference in shedding frequencies between the inner and outer cylinders results in a beat-like change in time-histories of lift. The inner cylinder St locks-in to the outer cylinder, being modified and reduced. As a result, the four cylinders again possess an identical $St = 0.194$.

3.3. Total time-averaged drag force

It is of interest to know how the time-averaged drag force on the four cylinders varies with g^* . The total drag force C_{D1-4} on the four cylinders is obtained by adding drag forces of the individual cylinders. It is presented as $C_{D1-4}/4C_{D0}$ in Fig. 13, where C_{D0} is the drag force on a single isolated cylinder. $C_{D1-4}/4C_{D0}$ rises with a decrease in g^* and reaches a maximum of 2.36 when the cylinders are in contact ($g^* = 0.0$). That is, the total drag on four cylinders (fingers) in contact is 2.36 times larger than that for a very large spacing. With a decrease in g^* , the increase in drag is dramatic ($1.68 \leq C_{D1-4}/4C_{D0} \leq 2.36$), significant ($1.4 < C_{D1-4}/4C_{D0} < 1.68$), and mild ($1.29 \leq C_{D1-4}/4C_{D0} < 1.4$) in the range $g^* \leq 0.25$, $0.25 < g^* < 1.0$ and $1.0 \leq g^* < 2.0$, respectively, corresponding to the single bluff-body, flip-flopping and quasi-interlocked flows. The relationship between $C_{D1-4}/4C_{D0}$ and g^* can be represented by a best fit curve equation, coefficients obtained using least square method, as follows:

$$\frac{C_{D1-4}}{4C_{D0}} = 1.0 + 0.51e^{-0.26g^*} + 0.85e^{-6g^*}.$$

The solid line in Fig. 13 represents the above equation. As $g^* \rightarrow \infty$, the equation gives $C_{D1-4}/4C_{D0} = 1.0$, satisfying that each of the cylinders behaves as a single isolated cylinder at a large g^* .

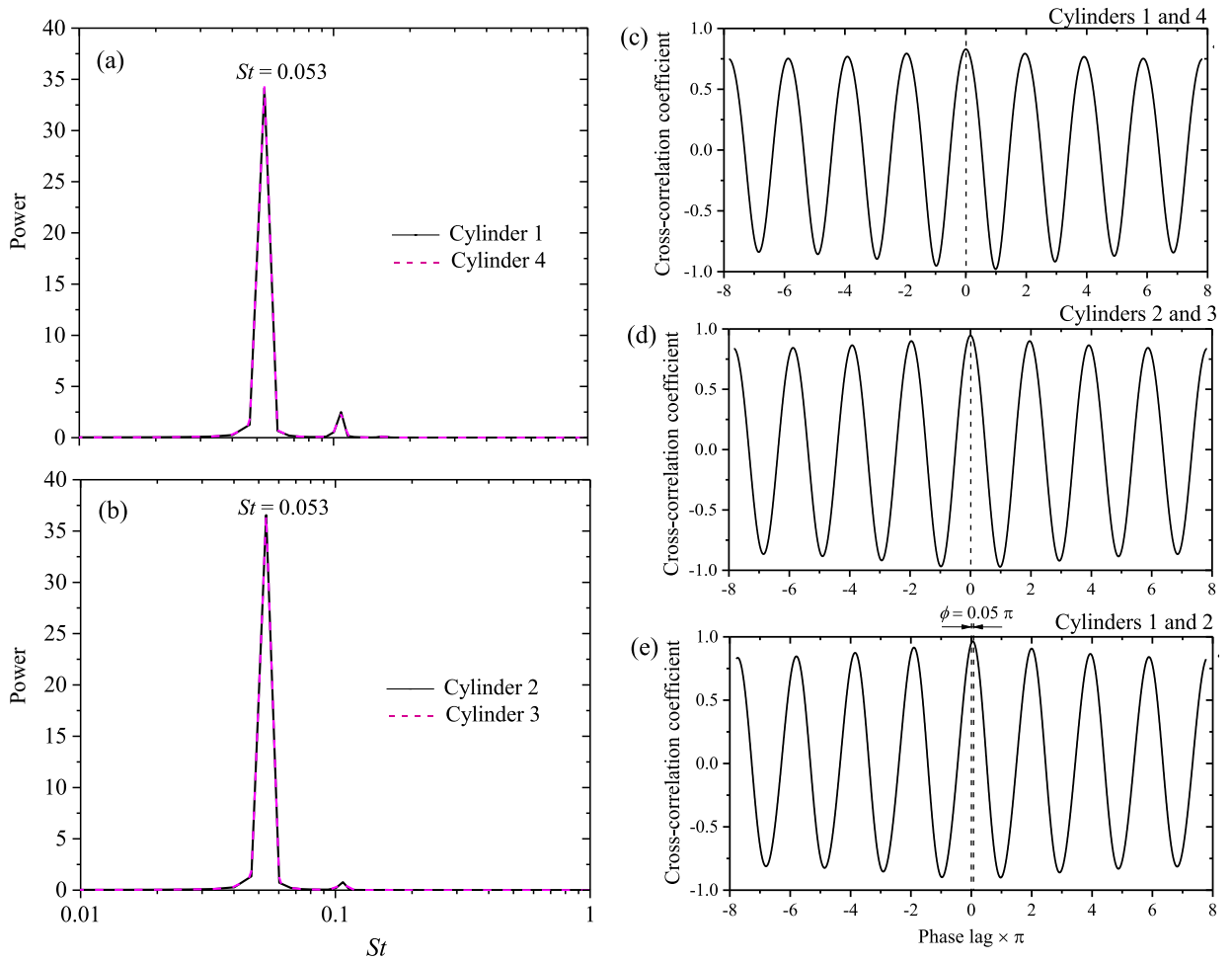


Fig. 11. (a, b) Power spectral density functions of fluctuating lift coefficients. (c, d, e) Cross correlation coefficient between fluctuating lift forces. The phase lag is calculated based on $St = 0.053$. $g^* = 0.25$. Single bluff-body flow.

4. Conclusions

A low-Reynolds number ($Re=100$) flow around four side-by-side circular cylinders is investigated with a change in normalized gap g^* from 0.0 to 2.0. Vorticity patterns, shedding frequencies, drag and lift forces are extracted and presented. Depending on g^* and features of the wake, the flow can be classified into four regimes: single bluff-body, flip-flopping, quasi-interlocked, and interlocked flows appearing at $g^* \leq 0.25$, $0.25 < g^* < 1.0$, $1.0 \leq g^* < 2.0$, and $g^* \geq 2.0$, respectively.

Regardless of which flow regime, the outer cylinders experience the identical C_D . So do the two inner cylinders. The C_D of the inner cylinders is, however, larger than that of the outer cylinders. The trend is the opposite for C_L and C'_L , being larger for outer cylinders. While the larger C_D is attributed to the fact that the inner cylinders are largely accompanied by narrow wakes with smaller formation length, the larger C_L and C'_L for outer cylinders are contributed to by the strong vortex shedding from the freestream sides. St is identical ($St \approx 0.05$) for the four cylinders in single body flow, different for the outer and inner cylinders in flip-flopping and quasi-interlocked flows, and again identical for interlocked flow. The difference in shedding frequencies between inner and outer cylinders results in a beat-like change in time-histories of lift. The vortex sheddings from the cylinders are highly correlated for interlocked flow, the cross-correlation coefficient being ≈ 1.0 between fluctuating lift of the cylinders. The phase lag between vortex sheddings from the outer cylinders is zero; so is that from the inner cylinders. For quasi-interlocked flow, the correlation coefficient between the two outer cylinders is smaller than 1.0 because of the inner cylinder interaction to the outer cylinders. On the contrary, the more interaction of the outer cylinders to the inner cylinders further deteriorates the correlation coefficient for the inner cylinders. Further degradation of the correlation coefficient occurs for flip-flopping flow, while a drastic improvement of the correlation coefficient succeeds for single body flow.

The single bluff-body flow is characterized by a hefty total drag force ($1.68 \leq C_{D1-4}/4C_{D0} \leq 2.36$) and a single wake behind the four cylinders. Prevailing wide and narrow wakes behind the cylinders, flip-flopping from one to the other randomly, exemplify the flip-flopping flow. The total drag force is still significant ($1.4 < C_{D1-4}/4C_{D0} < 1.68$), but smaller than that in the single bluff-body flow. A further smaller drag force ($1.29 \leq C_{D1-4}/4C_{D0} < 1.4$) prevails in the quasi-interlocked flow where the sheddings from the

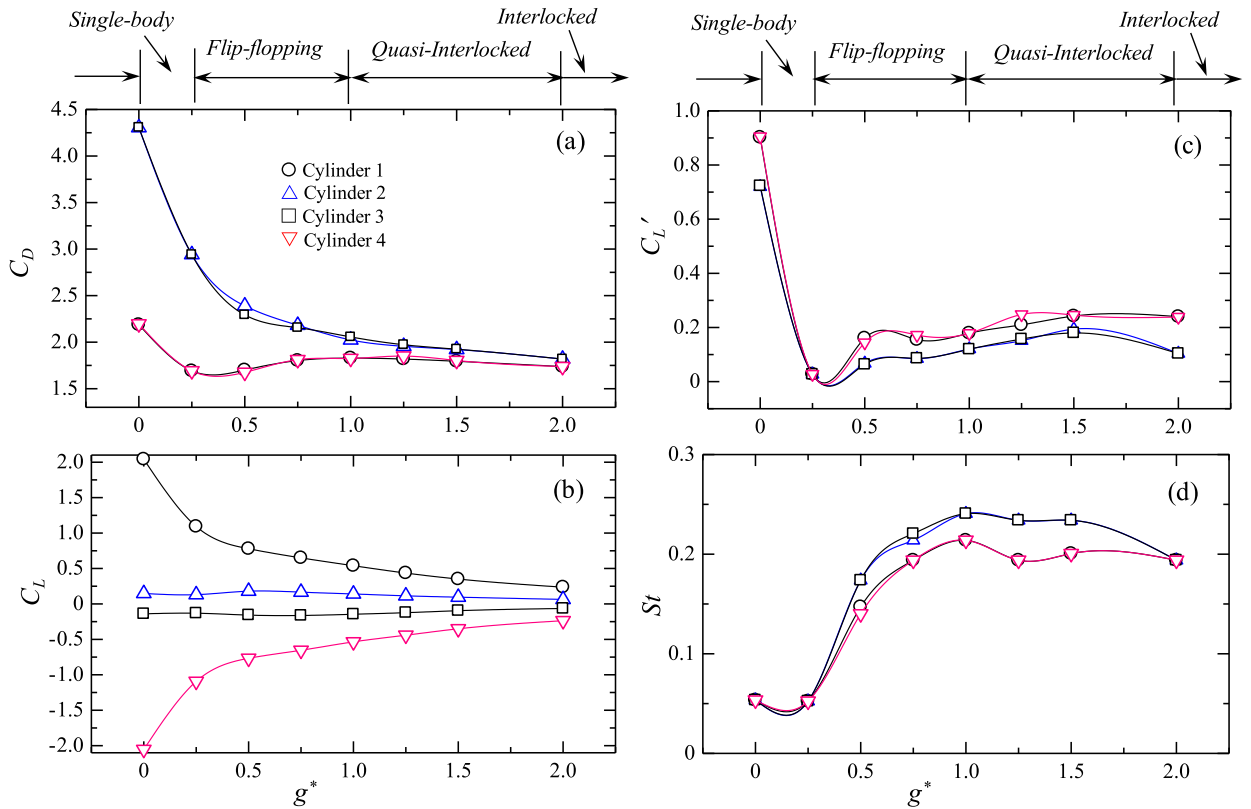


Fig. 12. Dependence on g^* of (a) time-averaged drag coefficient C_D , (b) time-averaged lift coefficient C_L , (c) fluctuation lift coefficient, and (d) Strouhal number St of the individual cylinders.

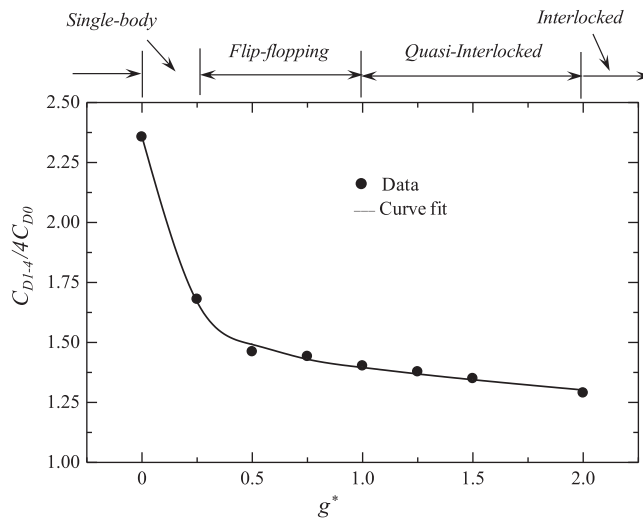


Fig. 13. Variation in the total time-averaged drag on four cylinders against g^* .

outer cylinders are interlocked inphase and those from the inner cylinders are in antiphase, with a higher shedding frequency appearing for the latter. The interlocked flow features the sheddings from all cylinders occurring in an inphase fashion with an identical frequency.

Acknowledgments

Alam wishes to acknowledge the supports given to him from National Natural Science Foundation of China through Grant 11672096 and from Research Grant Council of Shenzhen Government through grants QQCX2014052114423867 and

JCYJ20160531191442288. Hourigan acknowledges the support of the Australian Research Council's *Discovery Projects* funding scheme (project number DP150102879). The contributions of Xu Guoqing to the simulation are also gratefully acknowledged.

References

- Afgan, I., Kahil, Y., Benhamadouche, S., Sagaut, P., 2011. Large eddy simulation of the flow around single and two side-by-side cylinders at subcritical Reynolds numbers. *Phys. Fluids* 23, 075101.
- Alam, M.M., 2016. Lift forces induced by the phase lag between the vortex sheddings from two tandem bluff bodies. *J. Fluids Struct.* 65, 217–237.
- Alam, M.M., Zhou, Y., 2007. Flow around two side-by-side closely spaced circular cylinders. *J. Fluids Struct.* 23, 799–805.
- Alam, M.M., Zhou, Y., 2013. Intrinsic features of flow around two side-by-side square cylinders. *Phys. Fluids*, 25.
- Alam, M.M., Moriya, M., Sakamoto, H., 2003. Aerodynamic characteristics of two side-by-side circular cylinders and application of wavelet analysis on the switching phenomenon. *J. Fluids Struct.* 18, 325–346.
- Alam, M.M., Zhou, Y., Wang, X.W., 2011. The wake of two side-by-side square cylinders. *J. Fluid Mech.* 669, 432–471.
- Bearman, P.W., Wadcock, A.J., 1973. The interaction between a pair of circular cylinders normal to a stream. *J. Fluid Mech.* 61, 499–511.
- Bourguet, R., Jacon, L., 2014. Flow-induced vibrations of a rotating cylinder. *J. Fluid Mech.* 740, 343–380.
- Braza, M., Chassaing, P., Ming, H.H., 1986. Numerical study and physical analysis of the pressure and velocity fields in the near wake of a circular cylinder. *J. Fluid Mech.* 165, 79–130.
- Carini, M., Giannetti, F., Auteri, F., 2014. On the origin of the flip–flop instability of two side-by-side cylinder wakes. *J. Fluid Mech.* 742, 552–576.
- Ding, H., Shu, C., Yeo, Y.O., Xu, D., 2007. Numerical simulation of flows around two circular cylinders by mesh-free least square-based finite difference methods. *Int. J. Numer. Method Fl.* 53, 305–332.
- Kamemoto, K., 1976. Formation and interaction of two parallel vortex streets. *Bull. JSME* 19, 283–290.
- Kang, S., Choi, H., Lee, S., 1999. Laminar flow past a rotating circular cylinder. *Phys. Fluids* 11, 3312–3321.
- Kim, H.J., Durbin, P.A., 1988. Investigation of the flow between a pair of circular cylinders in the flopping regime. *J. Fluid Mech.* 196, 431–448.
- Kim, S., Alam, M.M., 2015. Characteristics and suppression of flow-induced vibrations of two side-by-side circular cylinders. *J. Fluids Struct.* 54, 629–642.
- Kumada, M., Hiwada, M., Ito, M., Mabuchi, I., 1984. Wake interference between three circular cylinders arranged side by side normal to a flow. *Trans. JSME* 50, 1699–1707, (in Japanese).
- Kumar, S.R., Sharma, A., Agrawal, A., 2008. Simulation of flow around a row of square cylinders. *J. Fluid Mech.* 606, 369–397.
- Meneghini, J.R., Saltara, F., 2001. Numerical simulation of flow interference between two circular cylinders in tandem and side-by-side arrangements. *J. Fluids Struct.* 15, 327–350.
- Moretti, P.M., 1993. Flow-induced vibrations in arrays of cylinders. *Annu. Rev. Fluid Mech.* 25, 99–114.
- Norberg, C., 2003. Fluctuating lift on a circular cylinder: review and new measurements. *J. Fluids Struct.* 17, 57–96.
- Prasanth, T.K., Mittal, S., 2008. Vortex-induced vibrations of a circular cylinder at low Reynolds numbers. *J. Fluid Mech.* 594, 463–491.
- Sewatkar, C.M., Sharma, A., Agrawal, A., 2011. Simulation of flow across a row of transversely oscillating square cylinders. *J. Fluid Mech.* 680, 361–397.
- Shen, L., Chan, E.S., Lin, P., 2009. Calculation of hydrodynamic forces acting on submerged moving object using immersed boundary method. *Comput. Fluids* 38, 691–702.
- Shiels, D., Leonard, A., Roshko, A., 2001. Flow-induced vibration of a circular cylinder at limiting structural parameters. *J. Fluids Struct.* 15, 3–21.
- Sohankar, A., Norberg, C., Davidson, L., 1998. Low-Reynolds-number flow around a square cylinder at incidence: study of blockage, onset of vortex shedding and outlet boundary condition. *Int. J. Numer. Methods Fl.* 26, 39–56.
- Tong, F., Cheng, L., Zhao, M., An, H., 2015. Oscillatory flow regimes around four cylinders in a square arrangement under small and conditions. *J. Fluid Mech.* 769, 298–336.
- Williamson, C.H.K., 1991. 2-D and 3-D aspects of the wake of a cylinder, and their relation to wake computations. *Lect. Appl. Math.* 28, 719–751.
- Williamson, C.H.K., 1996. Vortex dynamics in the cylinder wake. *Annu. Rev. Fluid Mech.* 28, 477–539.
- Zdravkovich, M.M., 1977. Review of flow interference between two circular cylinders in various arrangements. *ASME J. Fluids Eng.* 99, 618–633.
- Zdravkovich, M.M., 1997. *Flow around Circular Cylinders. Volume I. Fundamentals.* Oxford Science Publications, New York.
- Zhao, M., Cheng, L., 2014. Two-dimensional numerical study of vortex shedding regimes of oscillatory flow past two circular cylinders in side-by-side and tandem arrangements at low Reynolds numbers. *J. Fluid Mech.* 751, 1–37.